J Physiol 587.23 (2009) pp 5739–5752

The Journal of Physiology

Extracellular ATP inhibits chloride channels in mature mammalian skeletal muscle by activating $P2Y_1$ receptors

Andrew A. Voss

Department of Physiology, David Geffen School of Medicine at UCLA, University of California at Los Angeles, CA 90095-1751, USA

ATP is released from skeletal muscle during exercise, a discovery dating back to 1969. Surprisingly, few studies have examined the effects of extracellular ATP on mature mammalian skeletal muscle. This electrophysiological study examined the effects of extracellular ATP on fully innervated rat levator auris longus using two intracellular microelectrodes. The effects of ATP were determined by measuring the relative changes of miniature endplate potentials (mEPPs) and voltage responses to step current pulses in individual muscle fibres. Exposure to ATP (20 μM) prolonged the mEPP falling phase by 31 ± 7.5% (values ± S.D., $n = 3$ fibres). Concurrently, the input resistance increased by 31 ± 2.0% and the time course of the voltage responses increased by 59 ± 3.0%. Analogous effects were observed using 2 and 5 μM ATP, and on regions distal from the neuromuscular junction, indicating that physiologically relevant levels of ATP enhanced electrical signalling over the entire muscle fibre. The effects of extracellular ATP were blocked by 200 μM anthracene-9-carboxylic acid, a chloride channel inhibitor, and reduced concentrations of extracellular chloride, indicating that ATP inhibited chloride channels. A high affinity agonist for P2Y receptors, 2-methylthioadenosine-5′-*O*-diphosphate (2MeSADP), induced similar effects to ATP with an EC_{50} of 160 ± 30 nM. The effects of 250 nM 2MeSADP were blocked by 500 nM MRS2179, a specific $P2Y_1$ receptor inhibitor, suggesting that ATP acts on $P2Y_1$ receptors to inhibit chloride channels. The inhibition of chloride channels by extracellular ATP has implications for muscle excitability and fatigue, and the pathophysiology of myotonias.

(Resubmitted 24 July 2009; accepted after revision 28 September 2009; first published online 5 October 2009)
Corresponding author A. A. Voss: California State Polytechnic University, Pomona, Biological Sciences, 3801 West Temple Avenue, Pomona, CA 91768-4032, USA. Email: aavoss@csupomona.edu

Abbreviations 9AC, anthracene-9-carboxylic acid; ADPβS, adenosine 5′-*O*-(2-thio)diphosphate; ATPγS, adenosine 5′-*O*-(3-thio)triphosphate; ClC-1, muscle chloride channel; G_{Cl}, chloride conductance; mEPP, miniature end-plate potential; 2MeSADP, 2-methylthioadenosine-5′-*O*-diphosphate; MRS2179, 2′-deoxy-N^6-methyladenosine 3′,5′-biphosphate; NMJ, neuromuscular junction; NPS, normal physiological saline; P2X, ionotropic purinergic receptor; P2Y, metabotropic purinergic receptor; R_{in}, input resistance; R_m, membrane resistance.

Introduction

In 1969, Forrester & Lind demonstrated that the level of ATP in blood passing through human skeletal muscle increased during exercise from 300 nM in the arterial inflow to 10 μM in the venous effluent (Forrester & Lind, 1969). Even in blood flowing through resting muscle, the level of ATP was shown to increase from 300 nM to 1 μM (Forrester & Lind, 1969). Subsequently, it has been demonstrated that ATP is released from skeletal muscle fibres and the presynaptic terminal of the neuromuscular junction (Silinsky, 1975; Smith, 1991; Santos *et al.* 2003; Sandonà *et al.* 2005;Burnstock, 2007). Other reports have demonstrated that ATP affects biological activity by directly binding to metabotropic P2Y or ionotropic P2X receptors, as well as indirectly at P1 receptors through its metabolite, adenosine (Burnstock, 2007).

Previous examinations of the effects of extracellular ATP on skeletal muscle have used either native tissue (e.g. amphibian or chicken muscle) or cultured cells (Redman & Silinsky, 1994; Wells *et al.* 1995; Henning, 1997). Such studies demonstrate that ATP modulates the function of the acetylcholine receptor and K^+ channels (Lu & Smith, 1991; Henning, 1997; Henning *et al.* 1992; Thomas & Hume, 1993), and acts through $P2Y_1$ receptors in myotubes to regulate the expression of the acetylcholine receptor and acetylcholinesterase (Choi *et al.* 2003). Generally, however, the effects of extracellular ATP

DOI: 10.1113/jphysiol.2009.179275

in skeletal muscle are attributed to adenosine acting on inhibitory P1 receptors (Henning, 1997). Yet, few reports have examined the effects of extracellular ATP on mature mammalian muscle.

The aim of this study was to determine the effects of extracellular ATP on intact, fully innervated rat levator auris longus muscle. The effects of ATP were primarily examined near the neuromuscular junction. It was found that extracellular ATP prolonged the falling phase of the miniature endplate potentials (mEPPs). To determine the mechanism underlying the prolonged mEPP decay, the muscle membrane properties were determined by measuring the changes in membrane potential induced by steady current pulses. Extracellular ATP increased the input resistance and prolonged the time course of the steady voltage response. These effects of ATP resulted from extracellular ATP inhibiting Cl^- channels, which in mammalian muscle mediate 85% of the resting conductance (Palade & Barchi, 1977), by activating G protein-coupled $P2Y_1$ receptors. Physiologically, the large resting chloride conductance (G_{Cl}) in muscle influences the resting membrane potential, excitability and fatigue (Dulhunty, 1978; Cairns *et al.* 2004; van Emst *et al.* 2004; Dutka *et al.* 2008). Strong evidence indicates that the channel responsible for most of the G_{Cl} in muscle is ClC-1 (Steinmeyer *et al.* 1991*a*,*b*). Pathologically, mutations in ClC-1 underlie the hyperexcitability seen in Thomsen and Becker myotonias (Bryant & Morales-Aguilera, 1971; Steinmeyer *et al.* 1991*a*). By demonstrating that extracellular ATP inhibits muscle chloride channels, this study reveals an important purinergic signalling mechanism with broad implications for muscle physiology and pathophysiology.

Methods

Ethical approval

All animal procedures were performed in accordance with the policies of the University of California Chancellor's Committee on Animal Research and the guidelines for animal experimentation published by the *Journal of Physiology* (Drummond, 2009). Twenty-three Sprague–Dawley rats, aged 29–36 postnatal days, were anaesthetized by halothane inhalation and killed by cervical dislocation. Whole tissue rat levator auris longus was dissected and pinned out in a custom-designed Sylgard recording chamber. The tissue was maintained at room temperature (21°C) in a gassed (95% O_2 and 5% CO_2) normal physiological saline solution (NPS) composed of (in mM) 119 NaCl, 4 KCl, 1 $CaCl_2$, 4 $MgSO_4$, 1 NaH_2PO_4, 5 glucose, and 25 $NaHCO_3$. The pH of the gassed NPS solution was 7.2–7.4. For experiments in low external Cl^-, the tissue was maintained in a reduced Cl^- solution made by replacing the NaCl and KCl in the NPS with equimolar amounts of sodium and potassium methanesulfonate and was composed of (in mM) 119 $NaCH_3SO_3$, 4 KCH_3SO_3, 1.6 $CaCl_2$, 4 $MgSO_4$, 1 NaH_2PO_4, 5 glucose, and 25 $NaHCO_3$. This solution was also gassed in 95% O_2 and 5% CO_2, and had a pH of 7.2–7.4.

Experiments on frog (*Rana pipiens*) neuromuscular junctions were performed using a NPS composed of (in mM): 116 NaCl, 2 KCl, 1.8 $CaCl_2$, 1 $MgCl_2$, 10 Hepes, 1 $NaHCO_3$ and pH 7.4. Samples of cutaneous pectoris were kindly prepared by the laboratory of Dr Alan Grinnell. Frogs were anaesthetized with 0.1% tricaine methanesulfonate and killed by double pithing.

Electrophysiology

Muscle fibres were impaled with two aluminosilicate microelectrodes (Harvard Apparatus, Holliston, MA, USA), a voltage-recording electrode (10–20 MΩ) filled with 3 M KCl and a current-passing electrode (30–60 MΩ) filled with (in mM) 300 aspartate, 5 $MgCl_2$, 5 glutathione, 5 ATP dipotassium, 5 phosphocreatine disodium, 20 Mops and pH 7.2. To measure miniature endplate potentials (mEPPs) and determine the membrane characteristics, the electrodes were positioned 20–50 μm apart, with either electrode 20–100 μm from the presynaptic terminal. Neuromuscular junctions were identified with the aid of the membrane and synaptosomal fluorescent dye FM 1–43 (Invitrogen, Carlsbad, CA, USA) at 1 μM with an upright Olympus (Melville, NY, USA) BX50WI microscope. Epifluorescence was measured with a HQ470/40 X excitation filter, 500 nm dichroic mirror and HQ525/50 M emission filter. To determine the membrane characteristics in non-junctional regions, the electrodes were positioned 20–40 μm apart, approximately 5 mm from the presynaptic terminal.

The initial impaling of the electrodes caused a slight depolarization for each electrode, as observed by measuring the change in membrane potential upon impaling the second electrode. The resting membrane potential was adjusted to −80 to −95 mV with a current of −5 to −20 nA applied through the current-passing electrode. This current was held constant throughout the rest of the recording, except during the application of step current pulses. The recording was stopped if the resting membrane potential changed by ±10 mV. Recordings were made using an Axoclamp-2A amplifier (Molecular Devices, Sunnyvale, CA, USA), a BNC-2090 data acquisition board (National Instruments, Austin, TX, USA) and custom software (EVAN 1.2) written for LabView (courtesy of Dr Istvan Mody at UCLA). Data were low-pass filtered at 1 kHz with an 8-pole Bessel filter (Frequency Devices, Model 902, Ottawa, IL, USA) and acquired at 12.5 kHz.

Table 1. Summary of NMJ enhancement by ATP and related analogues

Agonist	No. of fibres	Maximum mean increase from NPS of: mEPP decay τ (%)	Input resistance (%)	Voltage response decay, τ_2 (%)
20 μM ATP	3	31 ± 8	31 ± 2	59 ± 3
20 μM ATPγS	3	42 ± 8	43 ± 8	78 ± 4
20 μM ADPβS	3	15 ± 6	20 ± 8	42 ± 13
10 μM 2MeSADP	3	36 ± 8	35 ± 1	73 ± 8

Data from individual muscle fibres were collected as described for Figs 1 and 2 by measuring the effects of agonist exposure on mEPPτ values, input resistance and the falling phase of the steady voltage response. These measurements were normalized by determining the percentage change from pre-exposure NPS levels. The values in Table 1 are the mean percentage changes $\pm$ standard deviation induced by agonist exposure in three muscle fibres.

Data acquisition and analysis

The responses over time were recorded continuously from individual fibres. Agonists and inhibitors were dissolved in the NPS or reduced Cl^- solutions and applied to the tissue using constant perfusion. The recording chamber was 1 ml and perfusion occurred at 10 ml min^{-1}. A solution change was considered complete after 1.5 min of perfusion. Except for measurements made in the presence of ATP and adenosine, the adenosine receptor antagonist, 8-cyclopentyl-1,3-dipropylxanthine (100 nM), was added to minimize the characteristic inhibitory effects of adenosine (Burnstock, 2007).

Throughout the recordings, mEPPs from 1–1.5 min periods, in different conditions, were detected and individually analysed for the frequency, amplitude, rise time and exponential decay using Mini Analysis (Synaptosoft, Fort Lee, NJ, USA). The average mEPP exponential decay values (mEPP$\tau \pm$ S.E.M.) from the 1–1.5 min periods were plotted as a function of the full recording time (mEPPs that were not fitted with an r^2 of at least 0.95 were excluded from analysis). Significant differences in the full time course of mEPP values were determined using one-way ANOVA with a significance level of 0.05 (using Microsoft Office Excel, Redmond, WA, USA). A conservative *post hoc* Scheffé test was used to determine which mEPPτ values significantly differed from levels in NPS (significance level of 0.05).

The membrane properties of the fibre were determined by measuring the changes in membrane potential induced by step current pulses applied through the current-passing electrode. The resulting steady voltage changes were analysed using SigmaPlot (Systat Software, San Jose, CA, USA). Passive cable properties were measured by using 100 nM tetrodotoxin and small current pulses (-5 to $+15$ nA). The average steady voltage change was plotted as a function of the applied current and a linear curve fit was used to determine the input resistance ($\pm$ standard error of curve fit) of the fibre. To determine the membrane time constants, the falling phase of the step voltage response was fitted with eqn (1):

$$y = y_0 + A_1 e^{-\frac{t}{\tau_1}} + A_2 e^{-\frac{t}{\tau_2}} + A_3 e^{-\frac{t}{\tau_3}} \quad (1)$$

Thus, from an individual muscle fibre, the effects of different conditions on mEPPs acquired during 1–1.5 min periods were measured concurrently with estimates of the fibre input resistance (R_{in}) and membrane time constants. mEPPs that occurred during a step voltage response were excluded from the analysis.

Since the baseline mEPP and membrane properties depend on the fibre diameter, the percentage changes of these properties in an individual fibre were determined and used to compare the responses in different fibres. The average percentage changes from multiple fibres are presented as mean $\pm$ S.D. (Table 1). Determining the percentage changes also allows comparisons of the magnitude of the effects in an individual fibre.

For instance, the R_{in} and membrane time constant are related to the membrane resistance (R_m) using one-dimensional cable theory as follows (Jack *et al.* 1983):

Definitions:

R_{in} = input resistance (steady voltage response/applied current)
r_m = membrane resistance per unit length of fibre
r_i = intracellular resistance per unit length of fibre
c_m = membrane capacitance per unit length of fibre
τ_m = membrane time constant
a = radius of fibre

Equations:

$$R_{in} = 0.5\sqrt{r_m r_i} \quad (2)$$

$$R_m = r_m(2\pi a) \quad (3)$$

$$\tau_m = r_m c_m \quad (4)$$

Then, from eqns (2) and (3), if r_i is constant:

$$R_{in} \propto \sqrt{r_m} \propto \sqrt{R_m} \quad (5)$$

and, from eqns (4) and (3), if c_m is constant:

$$\tau_m \propto r_m \propto R_m, \quad (6)$$

where $\propto$ is the proportionality symbol.

The EC_{50} ($\pm$ standard error of fit) for the effects of 2-methylthioadenosine-5′-*O*-diphosphate (2MeSADP) on the mEPP decay, R_{in} and τ_2 were determined as follows:

$$\frac{y}{y_{max}} = \frac{[2MeSADP]}{EC_{50} + [2MeSADP]}, \quad (7)$$

where $y =$ values of mEPP decay, R_{in} or τ_2.

Materials

Adenosine was purchased from Research Biochemical International (Natick, MA, USA); 2MeSADP from BioLog Life Science Institute (Bremen, Germany); and 2′-deoxy-N^6-methyladenosine 3′,5′-biphosphate (MRS2179) and 8-cyclopentyl-1,3-dipropylxanthine (DPCPX) were from Tocris Bioscience (Ellisville, MO, USA). All other chemicals were purchased from Sigma-Aldrich (St Louis, MO, USA) or Fisher Scientific (Pittsburgh, PA, USA).

Results

ATP effect on synaptic transmission

The effects of extracellular ATP on miniature endplate potentials (mEPPs) were determined on individual muscle fibres near the neuromuscular junction (NMJ). Figure 1*A* illustrates three representative mEPPs recorded in normal physiological saline (NPS) before the addition of ATP. The average time constant of decay of individual mEPPs (mEPPτ) recorded over a 1 min period was 2.8 ± 0.1 ms (mean $\pm$ S.E.M., $n = 39$) in NPS (Fig. 1*B*). Bath application of 20 μM ATP prolonged the falling phase of the mEPPs. Analysis of the decay phase indicated that the average mEPPτ was 3.9 ± 0.1 ms ($n = 44$) in response to ATP (Fig. 1*B*). After ATP washout, the mEPPτ reversed to 3.0 ± 0.1 ms ($n = 70$). Figure 2*A* illustrates the time course of the effects of 20 μM ATP on mEPPτ values. The gradual nature of the ATP reversal, occurring over 10–15 min, and the delay in reaching a maximum effect suggest a metabotropic effect.

The effects of ATP were also determined for the rising phase and frequency of the mEPPs. The average 10–90% rise time of the mEPPs was 0.6 ± 0.1 ms ($n = 39$) in NPS and 0.6 ± 0.1 ms ($n = 44$) in response to 20 μM ATP. The frequency was 1.10 Hz in NPS and 1.05 Hz during the maximum ATP effect. Thus, in contrast to the decay, there was no corresponding change in the rising phase or frequency of the mEPPs. Figure 1*B* suggests an increase in mEPP amplitude, which in NPS was 1.0 ± 0.1 mV ($n = 39$) and during the maximum ATP effect on mEPPτ was 1.1 ± 0.1 mV ($n = 44$). However, this change is uncertain because the brief, spatially localized nature of a mEPP often results in a non-uniform depolarization of the muscle fibre (Jack & Redman, 1971; Jack *et al.* 1983).

ATP effects on muscle membrane properties

To understand better the mechanism by which ATP induced the prolonged mEPPs, the resting membrane properties were measured by applying step current pulses from an intracellular microelectrode positioned 20–50 μm from the voltage-recording electrode. The resulting changes in membrane potential, as illustrated in Fig. 1*A* for the responses to +10 nA pulses, were less affected by non-uniform depolarization than mEPPs (Jack *et al.* 1983).

With the onset of the step current pulse, the membrane potential was driven to a new steady-state value, and with termination of the current pulse, returned to the original value. The voltage responses to a series of −4 to +10 nA current pulses in NPS are presented in Fig. 1*C*. These responses were recorded during the same period as the mEPPs used for the NPS condition in Fig. 1*B*. The input resistance (R_{in}), which is the ratio of the voltage change to the applied current ($\Delta V/\Delta I$), was 0.70 ± 0.01 MΩ in NPS (Fig. 1). In response to 20 μM ATP the R_{in} increased to 0.92 ± 0.01 MΩ (Fig. 1*D* and *E*). After washout, the R_{in} reversed to 0.78 ± 0.01 MΩ, which is illustrated in the full time course of the effects of 20 μM ATP on the fibre R_{in} (Fig. 2*B*). Since the specific membrane conductance (G_m) equals the reciprocal of the membrane resistance (R_m), it follows that G_m is proportional to $1/R_{in}^2$ ($G_m = 1/R_m \propto 1/R_{in}^2$, eqn (5)). Based on this, 20 μM ATP induced a relative decrease in G_m of approximately 42%.

The effects of ATP were also determined for the falling phase of the voltage response that resulted from termination of the step current pulse. Figure 1*F* illustrates the decay of the voltage response elicited by +10 nA pulses in NPS. The decay was well fitted by a triple exponential (eqn (1) in Methods), yielding fast ($\tau_1 = 0.3$–0.6 ms), medium ($\tau_2 = 2.8$–4.6 ms) and slow decay constants ($\tau_3 = 43$–93 ms) with fractional amplitudes of A_1 (0.3), A_2 (0.5–0.6) and A_3 (0.1), respectively. ATP strongly influenced τ_2, the largest fraction of the decay, increasing it from 2.8 ± 0.1 ms in NPS to 4.6 ± 0.1 ms in response to 20 μM ATP (Fig. 2*C*). The fast τ_1, because of its rapid nature and smaller fractional amplitude, was a less reliable indicator of ATP effects than τ_2. The slow τ_3, previously

characterized in muscle (Barry & Dulhunty, 1984), was also a less reliable indicator because of its small fractional amplitude. After washout of ATP, R_{in} and τ_2 reversed with the same time course as mEPPτ (Fig. 2*A*–*C*).

Figure 2*D* shows the effects of 20 μM ATP on mEPPτ, R_{in} and τ_2 expressed as percentage change to allow comparison of data from different muscle fibres. The maximum responses of other agonists that induced a similar effect to ATP at the NMJ are presented in Table 1. These agonists included the slowly hydrolysable ATP analogue adenosine 5′-*O*-(3-thio)triphosphate (ATPγS), the slowly hydrolysable ADP analogue adenosine 5′-*O*-(2-thio)diphosphate (ADPβS), and 2-methylthioadenosine-5′-*O*-diphosphate (2MeSADP).

Effects of ATP at lower concentrations

The effects of lower concentrations of ATP were also tested (Fig. 3*A*–*C*). Each concentration of ATP was applied after establishing a stable baseline in NPS. ATP (2 μM) prolonged the mEPP decay by 11% (Fig. 3*A*), R_{in} by 14% (Fig. 3*B*) and τ_2 by 25% (Fig. 3*C*); similar results were observed using 5 μM ATP (Fig. 3).

ATP inhibits chloride channels

A likely explanation for the increase in mEPPτ, R_{in} and τ_2 values elicited by extracellular ATP is a higher membrane resistance (R_m) resulting from ATP inhibiting

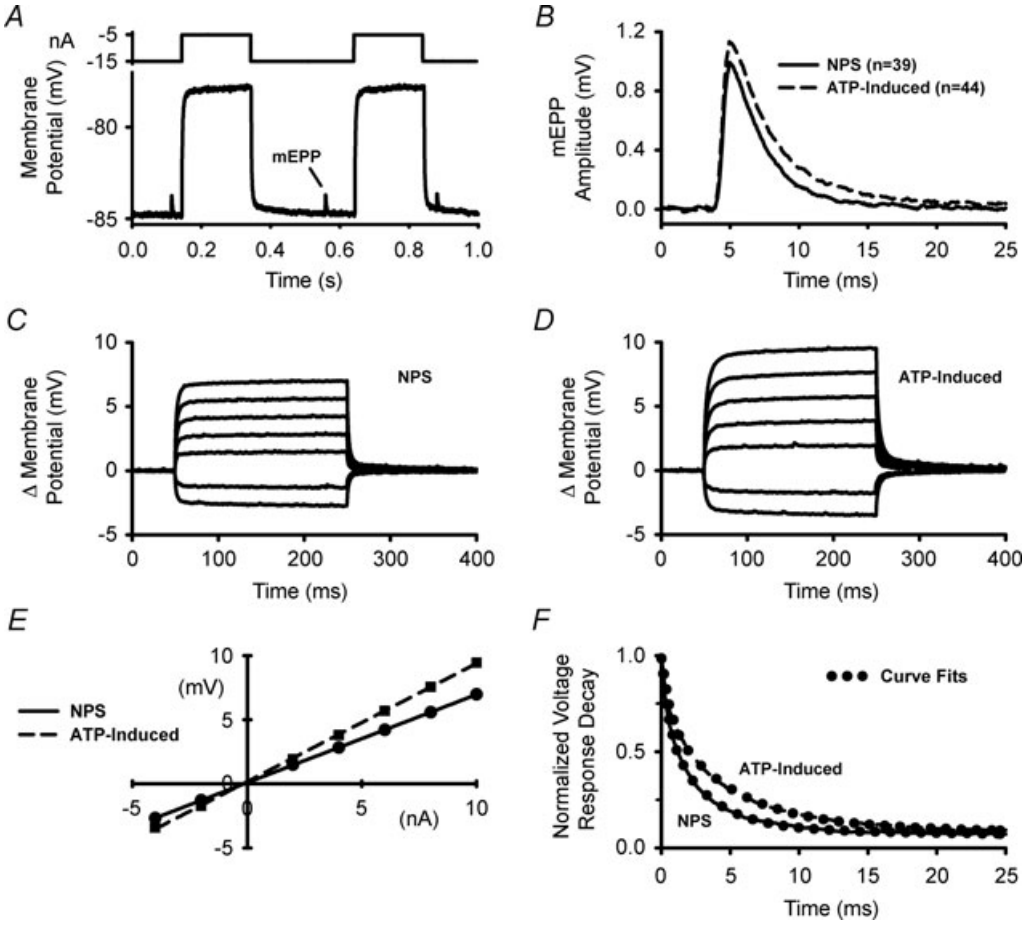

Figure 1. Effect of extracellular ATP on mEPPs and membrane properties
A, representative recording illustrating spontaneous mEPPs and voltage responses to 10 nA, 200 ms square pulses. The top panel illustrates the current applied through the current-passing electrode. *B*, average of 39 mEPPs in NPS (continuous line) and 44 mEPPs during the maximum response induced by 20 μM ATP (dashed line). *C* and *D*, the changes in membrane potential elicited by 2 Hz square current pulses of 10, 8, 6, 4, 2, −2 and −4 nA (each trace is the average of 7–12 responses) in NPS (*C*) and during the maximum response induced by 20 μM ATP (*D*). *E*, change in membrane potential (averaged from 150–230 ms in *C* and *D*) plotted as a function of current before ATP (continuous line) and during the maximum response induced by 20 μM ATP (dashed line). *F*, normalized decay of the average membrane potential changes induced by 10 nA pulses before application of ATP (continuous line) and during the maximum response induced by 20 μM ATP (dashed line). Each curve was fitted with an exponential decay (circles) using eqn (1) in Methods. Circles were used to identify the curve-fitted decay because of the tight overlap with the measured voltage decay. The data in this figure are all from the same muscle fibre.

Cl^- and/or K^+ channels. To determine if ATP inhibits Cl^- channels, the effects of the Cl^- channel blocker anthracene-9-carboxylic acid (9AC) were examined in the absence and presence of extracellular ATP (Fig. 4*A*–*C*). Figure 4*A* illustrates the time course of the effects of 200 μM 9AC on the average mEPPτ values. This concentration of 9AC produces near maximal inhibition of muscle Cl^- currents (Bryant & Morales-Aguilera, 1971; Bretag, 1987; Fahlke & Rüdel, 1995). Over a 1 min period in NPS, the average mEPPτ value was 3.4 ± 0.1 ms ($n = 106$), but after a 10 min exposure to 200 μM 9AC, it was 5.7 ± 0.1 ms ($n = 117$), an increase of 68% (Fig. 4*A*). Subsequent application of 20 μM ATP in the presence of 9AC did not significantly change the mEPPτ (5.5 ± 0.1 ms, $n = 140$) from the previous level in 9AC alone (Scheffé test: $P > 0.05$), suggesting that 9AC blocked the effect of ATP (Fig. 4*A*). Changes in mEPPτ, however, are not necessarily accurate indicators of changes in R_m. This is because, as stated above, the electrotonic spread associated with a mEPP often results in a non-uniform depolarization (Jack & Redman, 1971; Jack *et al.* 1983). Thus, mEPPs measured at distances less than the space constant decay faster than the time constant of the membrane (Fatt & Katz, 1951; Jack & Redman, 1971). Furthermore, the duration of the current that induces a mEPP influences its falling phase, with the rate of decay becoming faster as the current duration decreases (Jack & Redman, 1971; Jack *et al.* 1983).

Because voltage responses to step current pulses are more uniform, the effects of 9AC and ATP on the time courses of R_{in} and τ_2 from the same fibre were examined (Fig. 4*B* and *C*). In the presence of 200 μM 9AC, the R_{in} increased from 0.56 ± 0.01 MΩ to 1.15 ± 0.05 MΩ. This change in R_{in} is equivalent to a relative decrease in G_m of 76%, consistent with the 86% change in G_m observed by Bryant & Morales-Aguilera (1971) using 9AC (based on measurements of R_m). Subsequent application of 20 μM ATP produced no further increase in R_{in} (1.12 ± 0.03 MΩ) (Fig. 4*B*). For the falling phase of the step voltage response, 200 μM 9AC induced an increase in τ_2 from 2.6 ± 0.1 ms to 8.1 ± 0.1 ms (Fig. 4*C*). In the presence of 20 μM ATP and 200 μM 9AC, the τ_2 was 8.4 ± 0.1 ms (Fig. 4*C*).

Analogous experiments were performed on three separate muscle fibres from two additional rats with 200–500 μM 9AC and 20 μM ATPγS, the slowly hydrolysable analogue of ATP. In all three experiments, 9AC increased mEPPτ, R_{in} and τ_2, and blocked additional increases by ATPγS (representative time courses are presented in Supplemental Fig. 2, available online only).

The effects of 20 μM ATP were also examined in a reduced Cl^- solution, made by substituting NaCl

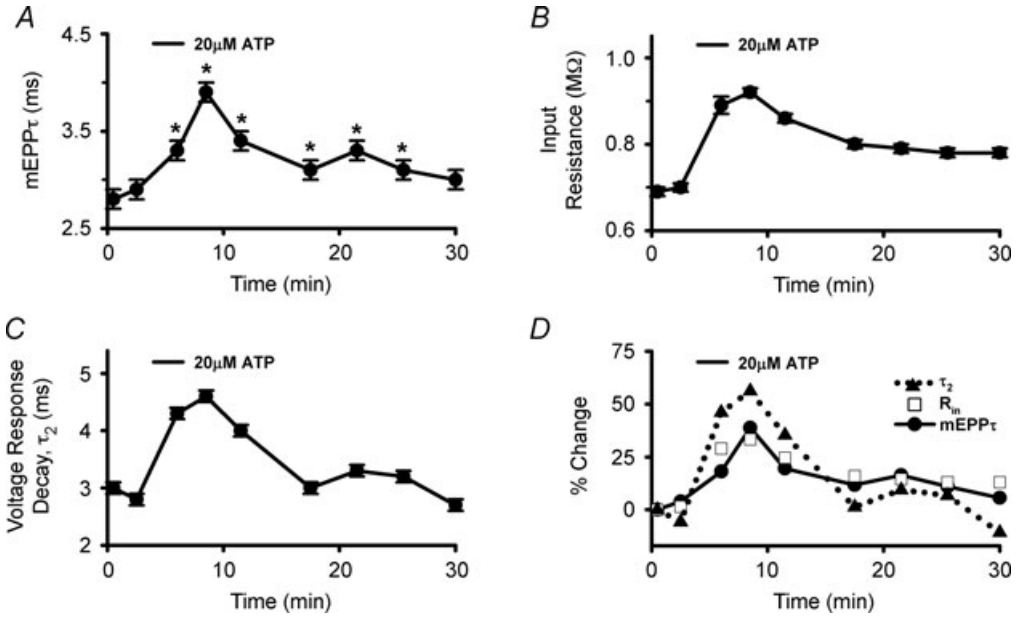

Figure 2. Time course of NMJ changes induced by 20 μM ATP
A, the exponential decay ($\tau \pm$ S.E.M.) of mEPPs before, during and after exposure to 20 μM ATP. Each value is the average of individually analysed mEPPs from a 1 min period recorded from the same muscle fibre. ANOVA indicated a significant difference in the mean mEPPτ values ($P < 0.05$, $F = 15.4$, $F_{crit} = 1.96$). The number of mEPPs analysed for each time point ranged from 17 to 70 and averaged 42. A *post hoc* Scheffé analysis was performed and * indicates a significant difference from before exposure to 20 μM ATP ($P < 0.05$). Similarly: *B*, measurements of input resistance ($R_{in} \pm$ standard error of curve fit) and *C*, the medium exponential decay ($\tau_2 \pm$ standard error of curve fit) of averaged responses to 10 nA injections (full curve-fitting results are presented in Supplemental Table 1, available online only). *D*, overlay of the percentage change in mEPPτ (●), R_{in} (□) and τ_2 (▲) from panels *A*, *B* and *C*. For presentation purposes, lines were used to connect mEPPτ data, but not those of R_{in}, which followed a similar time course.

and KCl with equimolar amounts of sodium and potassium methanesulfonate (Methods). This lowered the concentration of Cl^- from 125 mM in NPS to 3.2 mM in the reduced Cl^- solution. In the reduced Cl^- solution, there was not a significant difference in the time course of the mEPPτ values ($P > 0.05$, $F = 1.16$, $F_{crit} = 2.23$). This time course included mEPPτ values in the reduced Cl^- solution (5.4 ± 0.1 ms, $n = 92$), in response to 20 μM ATP (5.4 ± 0.1 ms, $n = 93$) and during washout of ATP (5.2 ± 0.1 ms, $n = 84$) (data not shown). Throughout the time course, the R_{in} ranged from 2.38 ± 0.02 MΩ to 2.48 ± 0.05 MΩ and the τ_2 ranged from 7.0 ± 0.1 ms to 8.0 ± 0.1 ms (data not shown). For R_{in} and τ_2, the highest values occurred in the reduced Cl^- solution before exposure to 20 μM ATP.

The ability of 9AC to induce increases in mEPPτ, R_{in} and τ_2 similar to those elicited by ATP and prevent additional increases by ATP, combined with the ability of a reduced Cl^- solution to block the effects of ATP, strongly suggest

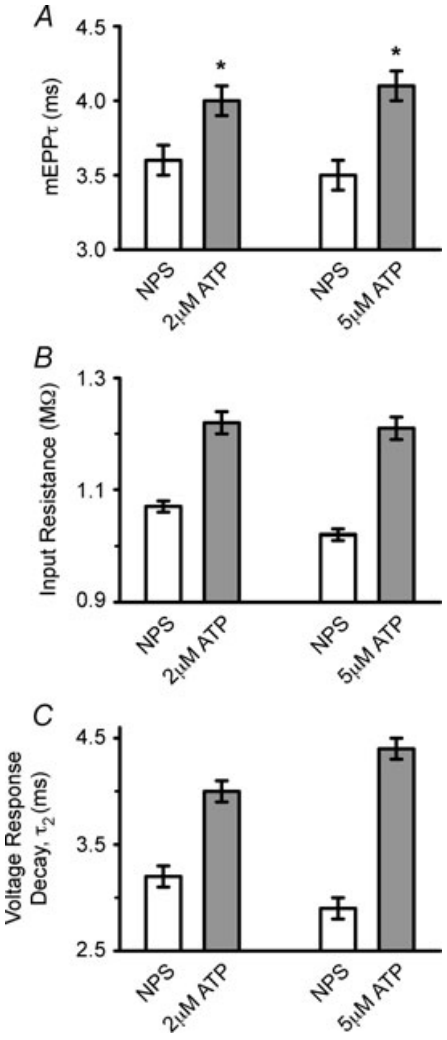

Figure 3. Low concentrations of extracellular ATP
A, the average exponential decay ($\tau \pm$ S.E.M.) of mEPPs in NPS and during the maximal responses to 2 and 5 μM ATP. These responses were obtained from the same fibre. ANOVA indicated a significant difference in the mEPPτ values from the full time course ($P < 0.05$, $F = 7.65$, $F_{crit} = 1.76$). A *post hoc* Scheffé analysis indicated a significant difference between the mEPPτ value in NPS ($n = 55$) and in response to 2 μM ATP ($n = 41$), as indicated by * ($P < 0.05$). Similarly, there was a significant difference between the mEPPτ value in NPS ($n = 58$) and in response to 5 μM ATP ($n = 52$) ($P < 0.05$). *B*, measurements of input resistance ($R_{in} \pm$ standard error of curve fit) in NPS and during the maximal responses to 2 and 5 μM ATP. *C*, the medium exponential decay ($\tau_2 \pm$ standard error of curve fit) of averaged responses to 10 nA injections in NPS and during the maximal responses to 2 and 5 μM ATP.

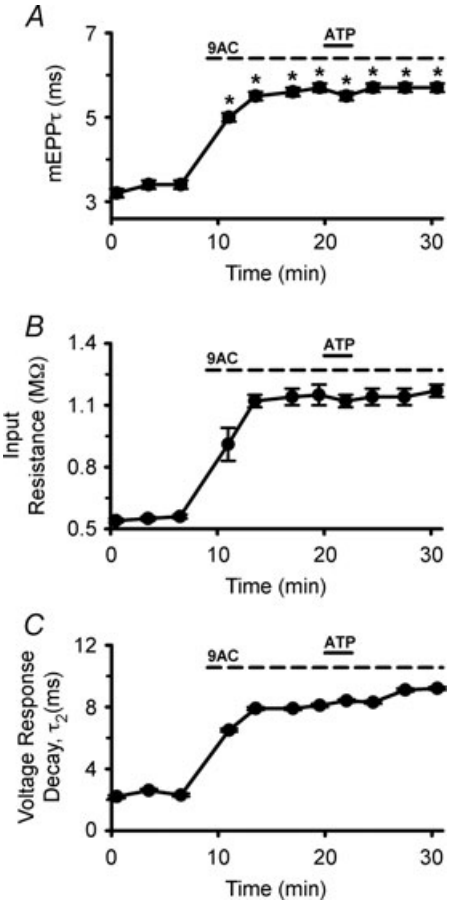

Figure 4. ATP inhibits chloride channels
A, the exponential decay ($\tau \pm$ S.E.M.) of mEPPs from an individual fibre before and during exposure to 200 μM 9AC (Cl^- channel blocker) and 200 μM 9AC + 20 μM ATP. ANOVA of these values indicates a significant difference ($P < 0.05$, $F = 92.2$, $F_{crit} = 1.84$). The number of mEPPs analysed for each time point ranged from 25 to 140 and averaged 91. A *post hoc* Scheffé analysis was performed and * indicates a significant difference from before exposure to 200 μM 9AC ($P < 0.05$). Similarly: *B*, measurements of the input resistance ($R_{in} \pm$ standard error of curve fit) and *C*, the medium exponential decay ($\tau_2 \pm$ standard error of curve fit) of averaged responses to 8 nA injections. Traces of the average mEPPs and step voltage responses in NPS, 9AC and 9AC + 20 μM ATP are presented in Supplemental Fig. 1*A–D*, available online only.

that extracellular ATP inhibits Cl^- channels in resting skeletal muscle. It is noteworthy that 9AC induced a small, 3–4 mV hyperpolarization of the resting membrane potential, which was not observed in response to ATP. This may indicate that ATP also regulates K^+ channels (Henning, 1997) or activates $P2X_4$ receptors that were recently identified in the transverse tubular system by confocal immunofluorescence (Sandonà *et al.* 2005).

Changing the resting conductance of Cl^- or K^+ may also alter the ionic and osmotic homeostasis of muscle and thus affect the fibre diameter and cytosolic resistance. To assess this, fibre diameters were measured optically. A fibre used to measure responses to 20 μM ATP was 32 μm in diameter before, during and 7 min after exposure to 20 μM ATP. Furthermore, three adjacent fibres averaged 28 μm in diameter before, during and 7 min after exposure to 20 μM ATP. This is consistent with previous work that showed exposure to 100 μM 9AC decreased the membrane conductance without changing the fibre diameter (Bryant & Morales-Aguilera, 1971). A stable fibre diameter suggests the cytosolic resistance was constant during the responses to ATP and that an increase in the R_m alone may account for the increased mEPPτ, R_{in} and τ_2. Assuming a constant cytosolic resistance, the percentage increase of τ_2 is greater than R_{in} because the decay is proportional to R_m (eqn (6), Methods), whereas R_{in} is proportional to the $\sqrt{R_m}$ (eqn (5), Methods).

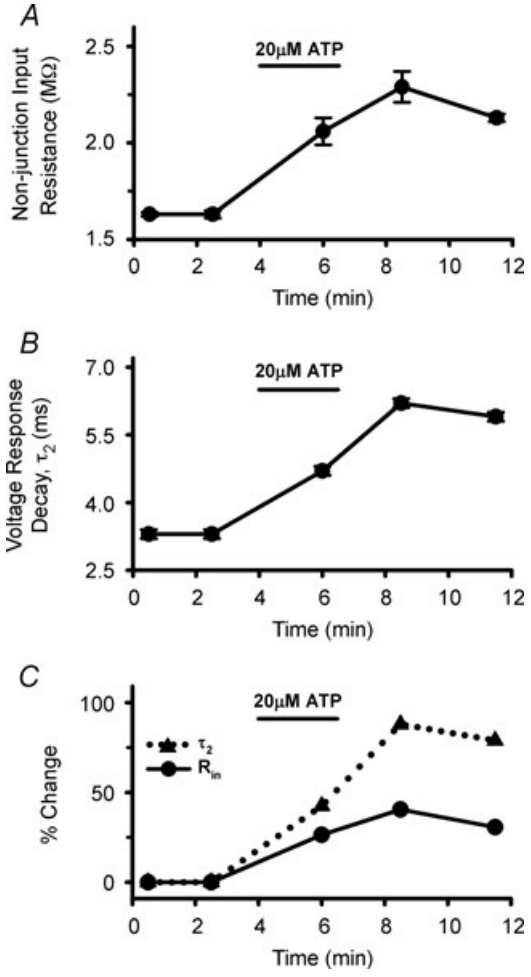

Figure 5. Non-junctional responses to ATP
A, measurements of R_{in} ($\pm$ standard error of curve fit) before, during and after exposure to 20 μM ATP. *B*, similarly, the medium exponential decay ($\tau_2 \pm$ standard error of curve fit) of averaged responses to 10 nA injections. *C*, overlay of the percentage change in R_{in} (●), and τ_2 (▲) from panels *A* and *B*.

Localization of the ATP effects

To examine the localization of the effect of extracellular ATP on Cl^- channels, responses to step current pulses were measured in non-junctional regions, approximately 5 mm from the endplate (Fig. 5*A*–*C*). At these distances, the diffusion of cytosolic signalling molecules from the NMJ would take hours. In response to 20 μM ATP, the non-junctional R_{in} increased from 1.63 ± 0.01 MΩ to 2.29 ± 0.08 MΩ (Fig. 5*A*) and the τ_2 of the voltage response falling phase increased from 3.3 ± 0.1 ms to 6.2 ± 0.1 ms (Fig. 5*B*). The normalized increases in the non-junctional R_{in} and τ_2 for this fibre were 40% and 88%, respectively (Fig. 5*C*). These data suggest that ATP responses were induced in non-junctional muscle and at the NMJ over the same time course.

ATP receptor identification and maximum effect

The effects of extracellular ATP, particularly at the NMJ, are often attributed to adenosine-activating P1 receptors (Henning, 1997). This was tested by measuring the response to adenosine. Before, during, and after exposure to 50 μM adenosine, the mEPPτ values ranged from 3.0 ± 0.1 ms ($n = 27$) to 3.3 ± 0.01 ms ($n = 40$) and there was not a significant difference in the full time course ($P > 0.05$, $F = 1.07$, $F_{crit} = 2.45$) (data not shown). R_{in} values ranged from 0.58 ± 0.01 to 0.63 ± 0.01 MΩ and the τ_2 ranged from 2.6 ± 0.1 to 3.0 ± 0.1 ms (data not shown). The highest values of mEPPτ, R_{in} and τ_2 occurred in NPS before exposure to 50 μM adenosine. Exposure to 50 and 100 μM adenosine was repeated in two additional fibres from two additional rats and in both experiments, no effects on mEPPτ, R_{in} or τ_2 were observed (data not shown).

The pharmacological profile of agonists in Table 1 suggests that the G protein-coupled $P2Y_1$, $P2Y_{12}$ or $P2Y_{13}$ receptors (Abbracchio *et al.* 2006) mediated the increases in mEPPτ, R_{in} and τ_2. Since 2MeSADP is known to activate P2Y receptors with high affinity (Abbracchio *et al.* 2006), a more definitive identification of the $P2Y_1$, $P2Y_{12}$ or $P2Y_{13}$ receptors requires demonstration that low concentrations of 2MeSADP induce the increases in mEPPτ, R_{in} and τ_2.

Thus, dose–response relationships were determined by exposing an individual fibre to concentrations of 2MeSADP from 100 nM to 1 μM and measuring mEPPτ, R_{in} and τ_2 (Fig. 6*A*–*F*). Exposure to each concentration was followed by at least 16 min of perfusion in NPS prior to the application of subsequent concentrations. Figure 6*A* illustrates the maximum effects of 100 nM to 1 μM 2MeSADP on average mEPPτ values, compared to pre-exposure NPS levels. Changes induced by 100, 250 and 500 nM, and 1 μM 2MeSADP were 11, 20, 25 and 26%, respectively (Fig. 6*B*). The mEPPτ values increased in response to 2MeSADP with an EC_{50} of 160 ± 30 nM (Fig. 6*B* and eqn (7) in Methods). Concurrently, in the same fibre, 100, 250 and 500 nM, and 1 μM 2MeSADP induced increases in R_{in} by 9, 22, 32 and 36%, respectively (Fig. 6*C* and *D*). The increase of R_{in} induced by 2MeSADP occurred with an EC_{50} of 340 ± 90 nM (Fig. 6*D*). Similarly, the τ_2 of the voltage response decay increased in response to 100, 250 and 500 nM, and 1 μM 2MeSADP by 22, 31, 63 and 66%, respectively, and occurred with an EC_{50} of 370 ± 180 nM (Fig. 6*E* and *F*). The high affinity of the effect of 2MeSADP on mEPPτ, R_{in} and τ_2 supports the identification of $P2Y_1$, $P2Y_{12}$ or $P2Y_{13}$ receptors.

In a separate fibre, the specific $P2Y_1$ inhibitor, MRS2179, was used to discriminate between $P2Y_1$, $P2Y_{12}$ or $P2Y_{13}$ receptors by examining the ability of MRS2179 to block the effects of 2MeSADP (Czajkowski *et al.* 2004; Fumagalli *et al.* 2004). Figure 7*A* illustrates the time courses of the changes in mEPPτ, R_{in} and τ_2. The average mEPPτ value from a 1 min period in NPS was 3.4 ± 0.1 ms

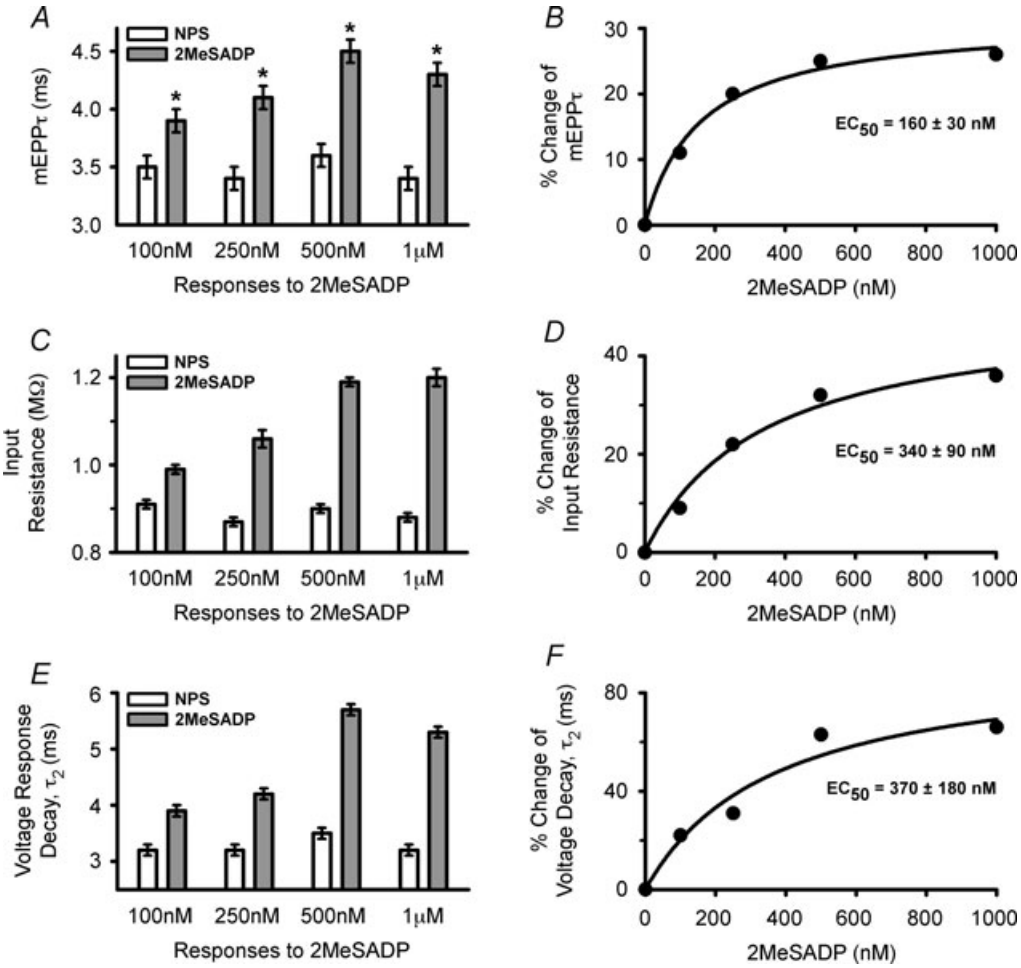

Figure 6. Dose–response of 2MeSADP

A, *C* and *E* illustrate the maximum effects of 2MeSADP (100 nM to 1 μM) on mEPPτ, R_{in} and τ_2, respectively. The effect for each concentration is plotted next to the pre-exposure NPS levels. All the responses were obtained from the same fibre. The percentage changes of the responses in *A*, *C* and *E* are plotted in *B*, *D* and *F*, respectively. The percentage changes were fitted with eqn (7) in the Methods to determine the EC_{50} values ($\pm$ standard error of curve fit). For the mEPPs, ANOVA of the full time course indicated a significant difference ($P < 0.05$, $F = 18.1$, $F_{crit} = 1.55$). The number of mEPPs analysed for each time point ranged from 29 to 81 and averaged 53. * in *A* indicates a significant difference from pre-exposure NPS levels (Scheffé test: $P < 0.05$).

($n = 46$) and in the presence of 500 nM MRS2179 alone was 3.5 ± 0.1 ms ($n = 26$). Addition of 250 nM 2MeSADP in the presence of 500 nM MRS2179 produced no change in mEPPτ (3.4 ± 0.1 ms, $n = 35$). However, after washing out the MRS2179 and 2MeSADP for 10 min in NPS, the addition of 250 nM 2MeSADP alone induced a significant increase in mEPPτ to 4.0 ± 0.1 ms ($n = 37$) ($P < 0.05$). Similar time courses were observed for R_{in} and τ_2 (Fig. 7*A*). In NPS, MRS2179 alone and MRS2179 + 2MeSADP, the R_{in} and τ_2 ranged from 0.67 ± 0.01 to 0.70 ± 0.1 MΩ, and 3.2 ± 0.1 to 3.5 ± 0.1 ms, respectively. In response to 250 nM 2MeSADP alone, R_{in} and τ_2 increased to 0.76 ± 0.01 MΩ and 4.3 ± 0.1 ms, respectively. The percentage increases of mEPPτ, R_{in} and τ_2 in response to 250 nM 2MeSADP alone were of magnitudes expected for a concentration near the EC_{50} (Fig. 7*A*). These experiments suggest that $P2Y_1$ is the ATP receptor mediating the increases in mEPPτ, R_{in} and τ_2.

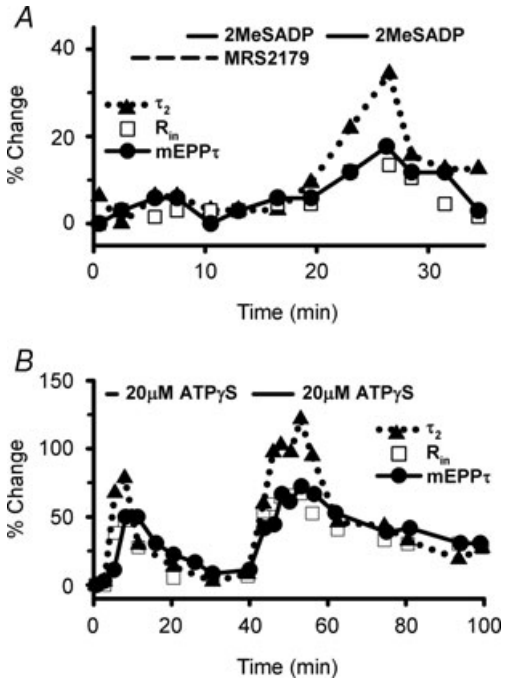

Figure 7. $P2Y_1$ receptor identification and maximum effect
A, overlay of the percentage change in mEPPτ (●), R_{in} (□) and τ_2 (▲) before, during and after exposure to 500 nM MRS2179 in the absence and presence of 250 nM 2MeSADP, with subsequent activation by 250 nM 2MeSADP alone. The initial values of mEPPτ, R_{in} and τ_2 in NPS were 3.4 ± 0.1 ms, 0.67 ± 0.01 MΩ and 3.4 ± 0.1 ms, respectively. *B*, overlay of the percentage change in mEPPτ (●), R_{in} (□) and τ_2 (▲) before, during and after normal exposure (2.5 min total perfusion time) and long exposure (10 min total perfusion time) of 20 μM ATPγS. The initial values of mEPPτ, R_{in} and τ_2 in NPS were 3.6 ± 0.1 ms, 0.76 ± 0.01 MΩ and 3.7 ± 0.1 ms, respectively. ANOVA on the non-normalized mEPPτ values used for *A* indicated a significant difference ($P < 0.05$, $F = 6.3$, $F_{crit} = 1.77$), the number of mEPPs analysed for each time point ranged from 26 to 58 and averaged 50. There was also a significant difference in the mEPPτ values used for *B* ($P < 0.05$, $F = 22.3$, $F_{crit} = 1.58$), the number of mEPPs analysed for each time point ranged from 25 to 93 and averaged 48. For presentation purposes, lines were not used to connect R_{in} (□) values in *A* and *B*.

To assess the magnitude of the effects mediated by $P2Y_1$ receptors, a fibre was exposed to 20 μM ATPγS for 2.5 min (duration normally used throughout this study) and 10 min (Fig. 7*B*). The average mEPPτ in NPS was 3.6 ± 0.1 ms ($n = 42$), which in response to the 2.5 min exposure significantly increased to 5.4 ± 0.2 ms ($n = 48$) ($P < 0.05$). After a 24 min washout, the mEPPτ reversed to 3.9 ± 0.2 ms ($n = 28$). A subsequent 10 min exposure to ATPγS induced a significant increase to 6.2 ± 0.2 ms ($n = 52$), which reversed to 4.6 ± 0.2 ms ($n = 50$) after 48 min of perfusion in NPS. Similar time courses were observed for R_{in} and τ_2 (Fig. 7*B*). The initial values of R_{in} and τ_2 in NPS were 0.76 ± 0.01 MΩ and 3.7 ± 0.1 ms, respectively. In response to the 10 min exposure of ATPγS, the R_{in} and τ_2 increased to 1.27 ± 0.02 MΩ and 8.2 ± 0.1 ms, respectively. The maximum increases in mEPPτ, R_{in} and τ_2 induced by the 10 min exposure relative to pre-exposure levels were 59, 61 and 116%, respectively. For the change in conductance, the maximum response to the 10 min exposure corresponds to a relative decrease of 64%. That the responses did not fully reverse after removal of ATPγS from the 10 min exposure suggests long-term potentiation. Exposures of ATP longer than 10 min may inhibit presynaptic vesicle release, as suggested in a recent study using mouse diaphragm (De Lorenzo *et al.* 2006). Comparing the percentage increases induced by a 10 min exposure to 20 μM ATPγS (Fig. 7*B*) and by 200 μM 9AC (Fig. 4) suggests that extracellular ATP inhibits a significant fraction of the resting G_{Cl} in mammalian skeletal muscle. This would include transverse tubular G_{Cl}, which constitutes the majority of the resting G_{Cl} (Palade & Barchi, 1977).

Mammalian, but not amphibian, skeletal muscle fibres possess a large t-tubular G_{Cl} (Dulhunty, 1979). Moreover, considerably higher doses and longer exposures to 9AC are required to induce myotonic behaviour in frogs compared to mammals (Bretag *et al.* 1980), suggesting that frogs have a reduced sensitivity to 9AC. These data raise the possibility that the effects of extracellular ATP on mammalian skeletal muscle might be less pronounced or even absent at the frog NMJ. To test this hypothesis, the response of the frog NMJ to 50 μM ATP was evaluated. Before, during, and after exposure to 50 μM ATP, the mEPPτ values were 6.8 ± 0.1 ms ($n = 137$), 6.8 ± 0.1 ms ($n = 154$) and 6.4 ± 0.1 ms ($n = 103$), respectively, and there was not a significant difference in the time course ($P > 0.05$, $F = 0.84$, $F_{crit} = 2.22$) (data not shown). Additionally, no apparent increases in R_{in} and τ_2 were observed (R_{in}: control, 1.86 ± 0.01 MΩ; ATP, 1.72 ± 0.01 MΩ; washout, 1.66 ± 0.02 MΩ; and τ_2: control, 7.7 ± 0.2 ms; ATP, 8.2 ± 0.1 ms; washout, 8.2 ± 0.2 ms) (data not shown).

Similar results were observed in two additional fibres, from one additional frog (data not shown).

Discussion

This study demonstrates that extracellular ATP directly enhances electrical signalling in mature, intact mammalian muscle by activating $P2Y_1$ receptors and hence, inhibiting Cl^- channels. The first observed effect of extracellular ATP was the prolongation of mEPPs. Because of the inherent variability of mEPPs measured at distances less than the space constant, step current pulses were applied to determine the mechanism underlying the prolonged mEPPs. The physiological significance of the prolonged mEPPs is unclear, as nerve stimulation in muscle is normally highly effective in generating action potentials. The $P2Y_1/Cl^-$ channel pathway was activated by 2 and 5 μM ATP, which have been shown to be physiologically relevant levels of extracellular ATP (Forrester & Lind, 1969; Li *et al.* 2008). The effects of extracellular ATP were measured at junctional and non-junctional regions of individual muscle fibres, suggesting that extracellular ATP inhibits Cl^- channels throughout the muscle fibre. This is potentially a substantial effect, because Cl^- channels in resting mammalian skeletal muscle are normally open and responsible for most of the resting conductance (Palade & Barchi, 1977). The channel probably inhibited by $P2Y_1$ is ClC-1, as this is responsible for most of the Cl^- conductance (G_{Cl}) in resting muscle (Steinmeyer *et al.* 1991*a*). Consistent with this idea, extracellular ATP inhibited a large fraction of the resting G_{Cl}. Specifically, during a 10 min exposure to the slowly hydrolysable ATPγS the resting membrane conductance decreased by 64%, which is near the 76% decrease in membrane conductance induced by 200 μM 9AC. Prior to this report, it was generally thought, based on studies in amphibian muscle, that extracellular ATP primarily produced inhibitory effects in developed muscle indirectly through adenosine. This study suggests that the stimulatory ATP response might be unique to mammals, because it is observed in rat, but not frog, muscle.

The functional identification of $P2Y_1$ receptors in this study is consistent with previous reports that have identified $P2Y_1$ receptors in rat (Choi *et al.* 2001) and human (Léon *et al.* 1996) skeletal muscle using immunohistochemistry and Northern analysis (Abbracchio *et al.* 2006; Burnstock, 2007). $P2Y_1$ receptors often exert biological effects by activating phospholipase C, which mediates the release of diacylglycerol and InsP_3, resulting in activation of protein kinase C (PKC) (Abbracchio *et al.* 2006). This mechanism is an initial candidate for the $P2Y_1/Cl^-$ channel pathway, as the InsP_3 signalling components are present in muscle (Vergara *et al.* 1985) and activation of PKC has been shown to inhibit Cl^- channels in rat skeletal muscle (Tricarico *et al.* 1991). Moreover, activation of PKC by 4β-phorbol esters attenuates ClC-1 Cl^- current in HEK293 cells heterologously expressing human ClC-1 (Rosenbohm *et al.* 1999).

This report provides the first evidence that extracellular ATP can act on $P2Y_1$ receptors to inhibit chloride channels. Other reported interactions of $P2Y_1$ receptors involve stimulating the chloride channel activity of the cystic fibrosis transmembrane conductance regulator (CFTR) and activating volume-sensitive chloride currents (Darby *et al.* 2003; Guerra *et al.* 2004). Studies in renal epithelial cells suggest that $P2Y_1$ receptor-mediated activation of PKC stimulates CFTR via potentiation of the protein kinase A pathway (Guerra *et al.* 2004). In astrocytes, the mechanism linking $P2Y_1$ receptors to volume-sensitive chloride currents was not identified; however, it was suggested that a $[Ca^{2+}]$-independent isoform of PKC might be involved (Darby *et al.* 2003). Finally, in biliary epithelial cells, it was recently reported that mechanosensitive ATP release activates Cl^- currents via P2Y receptors (Woo *et al.* 2008).

This study also reveals a novel regulatory mechanism of skeletal muscle Cl^- channels. Other factors known to regulate skeletal muscle Cl^- channels include pH and intracellular ATP. It has long been known that a decrease in pH inhibits muscle Cl^- channels (Hutter & Warner, 1967; Palade & Barchi, 1977). More specifically, analysis of heterologously expressed ClC-1 channels indicates that lowering the extracellular pH attenuates deactivating inward currents, but enhances steady-state currents (Rychkov *et al.* 1996). By contrast, when intracellular pH is decreased heterologously expressed ClC-1 Cl^- currents are inhibited because the voltage dependence of the common gate is shifted to more positive potentials (Bennetts *et al.* 2007). Interestingly, intracellular ATP inhibits ClC-1 by a similar mechanism (Bennetts *et al.* 2005), while the effects of intracellular ATP are enhanced by intracellular acidosis (Bennetts *et al.* 2007). The ability of intracellular ATP to inhibit muscle Cl^- channels suggests that at times of low metabolic stress, chloride conductance is reduced and muscle excitability is increased (Bennetts *et al.* 2005). However, a study using the *Xenopus* oocytes expression system demonstrated that intracellular ATP, even in acidic conditions, did not affect ClC-1 (Zifarelli & Pusch, 2008). It is unclear whether the $P2Y_1/Cl^-$ channel pathway identified here using extracellular ATP and mature muscle will clarify these contradictory finding for ClC-1 in different heterologous expression systems, but the results of this study do introduce an additional regulatory mechanism to consider in future studies of ClC-1 Cl^- channel function. During exercise, increases in extracellular ATP and decreases in pH might both reduce chloride conductance and increase muscle excitability.

Physiologically, the large resting G_{Cl} influences excitability, as mutations in ClC-1 result in the hyper-excitable states of Thomsen and Becker myotonias (Bryant & Morales-Aguilera, 1971; Steinmeyer *et al.* 1991*a*) and low extracellular Cl^- decreases the electrical stimulation required to achieve maximum twitch force (van Emst *et al.* 2004). Considering the role of G_{Cl} in muscle excitability and that extracellular ATP rises during exercise, it is possible that the $P2Y_1/Cl^-$ channel pathway contributes to the exercise-exacerbated stiffness associated with paramyotonia congenita (Ryan *et al.* 2007). Cl^- channels also help maintain the resting membrane potential (Hodgkin & Horowicz, 1959; Dulhunty, 1978). This function is thought to be important in preventing muscle fatigue, whereby G_{Cl} prevents depolarization of the transverse tubular system as extracellular K^+ increases during high-frequency stimulation (Dutka *et al.* 2008; van Emst *et al.* 2004). Consistent with this idea, Cairns *et al.* (2004) demonstrated that extracellular Cl^- protects isolated mammalian muscle fibres against fatigue. In contrast, it has been proposed that reducing G_{Cl} will help to prevent muscle fatigue during conditions of elevated interstitial K^+, because Na^+ currents will have less resting leak current to overcome during action potential propagation (Mohr *et al.* 2004; Pedersen *et al.* 2004; de Paoli *et al.* 2007). The effect of Cl^- channels on muscle fatigue might therefore depend on which of the many cellular mechanisms is inducing fatigue.

In summary, this study identifies a novel purinergic signalling mechanism in mammalian skeletal muscle that has been unrecognized for 40 years. Specifically, physiologically significant levels of extracellular ATP inhibit Cl^- channels by activating $P2Y_1$ receptors. The $P2Y_1/Cl^-$ channel pathway is a new regulatory mechanism of mammalian Cl^- channels, an important discovery because ATP is released from skeletal muscle during exercise. Based on the role of Cl^- channels, the activation of $P2Y_1$ receptors has implications for skeletal muscle excitability and fatigue, and the pathophysiology of myotonias.

References

Abbracchio MP, Burnstock G, Boeynaems JM, Barnard EA, Boyer JL, Kennedy C, Knight GE, Fumagalli M, Gachet C, Jacobson KA & Weisman GA (2006). International union of pharmacology LVIII: update on the P2Y G protein-coupled nucleotide receptors: from molecular mechanisms and pathophysiology to therapy. *Pharmacol Rev* **58**, 281–341.

Barry PH & Dulhunty AF (1984). Slow potential changes in mammalian muscle-fibres during prolonged hyperpolarization: transport number effects and chloride depletion. *J Membr Biol* **78**, 235–248.

Bennetts B, Parker MW & Cromer BA (2007). Inhibition of skeletal muscle ClC-1 chloride channels by low intracellular pH and ATP. *J Biol Chem* **282**, 32780–32791.

Bennetts B, Rychkov GY, Ng HL, Morton CJ, Stapleton D, Parker MW & Cromer BA (2005). Cytoplasmic ATP-sensing domains regulate gating of skeletal muscle ClC-1 chloride channels. *J Biol Chem* **280**, 32452–32458.

Bretag AH (1987). Muscle chloride channels. *Physiol Rev* **67**, 618–724.

Bretag AH, Dawe SR & Moskwa AG (1980). Chemically-induced myotonia in amphibia. *Nature* **286**, 625–626.

Bryant SH & Morales-Aguilera A (1971). Chloride conductance in normal and myotonic muscle fibres and action of monocarboxylic aromatic acids. *J Physiol* **219**, 367–383.

Burnstock G (2007). Physiology and pathophysiology of purinergic neurotransmission. *Physiol Rev* **87**, 659–797.

Cairns SP, Ruzhynsky V & Renaud JM (2004). Protective role of extracellular chloride in fatigue of isolated mammalian skeletal muscle. *Am J Physiol Cell Physiol* **287**, C762–C770.

Choi RCY, Man MLS, Ling KKY, Ip NY, Simon J, Barnard EA & Tsim KWK (2001). Expression of the $P2Y_1$ nucleotide receptor in chick muscle: its functional role in the regulation of acetylcholinesterase and acetylcholine receptor. *J Neurosci* **21**, 9224–9234.

Choi RCY, Siow NL, Cheng AWM, Ling KKY, Tung EKK, Simon J, Barnard EA & Tsim KWK (2003). ATP acts via $P2Y_1$ receptors to stimulate acetylcholinesterase and acetylcholine receptor expression: transduction and transcription control. *J Neurosci* **23**, 4445–4456.

Czajkowski R, Banachewicz W, Ilnytska O, Drobot LB & Barańska J (2004). Differential effects of $P2Y_1$ and $P2Y_{12}$ nucleotide receptors on ERK1/ERK2 and phosphatidylinositol 3-kinase signalling and cell proliferation in serum-deprived and nonstarved glioma C6 cells. *Br J Pharmacol* **141**, 497–507.

Darby M, Kuzmiski JB, Panenka W, Feighan D & MacVicar BA (2003). ATP released from astrocytes during swelling activates chloride channels. *J Neurophysiol* **89**, 1870–1877.

De Lorenzo S, Veggetti M, Muchnik S & Losavio A (2006). Presynaptic inhibition of spontaneous acetylcholine release mediated by P2Y receptors at the mouse neuromuscular junction. *Neuroscience* **142**, 71–85.

de Paoli FV, Overgaard K, Pedersen TH & Nielsen OB (2007). Additive protective effects of the addition of lactic acid and adrenaline on excitability and force in isolated rat skeletal muscle depressed by elevated extracellular K^+. *J Physiol* **581**, 829–839.

Drummond GB (2009). Reporting ethical matters in *The Journal of Physiology*: standards and advice. *J Physiol* **587**, 713–719.

Dulhunty AF (1978). Dependence of membrane potential on extracellular chloride concentration in mammalian skeletal muscle fibres. *J Physiol* **276**, 67–82.

Dulhunty AF (1979). Distribution of potassium and chloride permeability over the surface and T-tubule membranes of mammalian skeletal muscle. *J Membr Biol* **45**, 293–310.

Dutka TL, Murphy RM, Stephenson DG & Lamb GD (2008). Chloride conductance in the transverse tubular system of rat skeletal muscle fibres: importance in excitation–contraction coupling and fatigue. *J Physiol* **586**, 875–887.

Fahlke C & Rüdel R (1995). Chloride currents across the membrane of mammalian skeletal muscle fibres. *J Physiol* **484**, 355–368.

Fatt P & Katz B (1951). An analysis of the end-plate potential recorded with an intra-cellular electrode. *J Physiol* **115**, 320–370.

Forrester T & Lind AR (1969). Identification of adenosine triphosphate in human plasma and the concentration in the venous effluent of forearm muscles before, during and after sustained contractions. *J Physiol* **204**, 347–364.

Fumagalli M, Trincavelli L, Lecca D, Martini C, Ciana P & Abbracchio MP (2004). Cloning, pharmacological characterisation and distribution of the rat G-protein-coupled $P2Y_{13}$ receptor. *Biochem Pharmacol* **68**, 113–124.

Guerra L, Favia M, Fanelli T, Calamita G, Svelto M, Bagorda A, Jacobson KA, Reshkin SJ & Casavola V (2004). Stimulation of *Xenopus* P2Y1 receptor activates CFTR in A6 cells. *Pflugers Arch* **449**, 66–75.

Henning RH (1997). Purinoceptors in neuromuscular transmission. *Pharmacol Ther* **74**, 115–128.

Henning RH, Nelemans A, Vandenakker J & Denhertog A (1992). The nucleotide receptors on mouse C2C12 myotubes. *Br J Pharmacol* **106**, 853–858.

Hodgkin AL & Horowicz P (1959). The influence of potassium and chloride ions on the membrane potential of single muscle fibres. *J Physiol* **148**, 127–160.

Hutter OF & Warner AE (1967). The pH sensitivity of chloride conductance of frog skeletal muscle. *J Physiol* **189**, 403–425.

Jack JJB, Noble D & Tsien RW (1983). *Electric Current Flow in Excitable Cells*. Oxford University Press, Oxford.

Jack JJB & Redman SJ (1971). The propagation of transient potentials in some linear cable structures. *J Physiol* **215**, 283–320.

Léon C, Vial C, Cazenave JP & Gachet C (1996). Cloning and sequencing of a human cDNA encoding endothelial $P2Y_1$ purinoceptor. *Gene* **171**, 295–297.

Li JH, Gao ZH, Kehoe V, Xing JH, King N & Sinoway L (2008). Interstitial adenosine triphosphate modulates muscle afferent nerve-mediated pressor reflex. *Muscle Nerve* **38**, 972–977.

Lu Z & Smith DO (1991). Adenosine 5′-triphosphate increases acetylcholine channel opening frequency in rat skeletal muscle. *J Physiol* **436**, 45–56.

Mohr M, Nordsborg N, Nielsen JJ, Pedersen LD, Fischer C, Krustrup P & Bangsbo J (2004). Potassium kinetics in human muscle interstitium during repeated intense exercise in relation to fatigue. *Pflugers Arch* **448**, 452–456.

Palade PT & Barchi RL (1977). Characteristics of chloride conductance in muscle fibres of rat diaphragm. *J Gen Physiol* **69**, 325–342.

Pedersen TH, Nielsen OB, Lamb GD & Stephenson DG (2004). Intracellular acidosis enhances the excitability of working muscle. *Science* **305**, 1144–1147.

Redman RS & Silinsky EM (1994). ATP released together with acetylcholine as the mediator of neuromuscular depression at frog motor nerve endings. *J Physiol* **477**, 117–127.

Rosenbohm A, Rüdel R & Fahlke C (1999). Regulation of the human skeletal muscle chloride channel hClC-1 by protein kinase C. *J Physiol* **514**, 677–685.

Ryan AM, Matthews E & Hanna MG (2007). Skeletal-muscle channelopathies: periodic paralysis and nondystrophic myotonias. *Curr Opin Neurol* **20**, 558–563.

Rychkov GY, Pusch M, Astill DS, Roberts ML, Jentsch TJ & Bretag AH (1996). Concentration and pH dependence of skeletal muscle chloride channel ClC-1. *J Physiol* **497**, 423–435.

Sandonà D, Danieli-Betto D, Germinario E, Biral D, Martinello T, Lioy A, Tarricone E, Gastaldello S & Betto R (2005). The T-tubule membrane ATP-operated $P2X_4$ receptor influences contractility of skeletal muscle. *FASEB J* **19**, 1184.

Santos DA, Salgado AI & Cunha RA (2003). ATP is released from nerve terminals and from activated muscle fibres on stimulation of the rat phrenic nerve. *Neurosci Lett* **338**, 225–228.

Silinsky EM (1975). Association between transmitter secretion and release of adenine nucleotides from mammalian motor nerve terminals. *J Physiol* **247**, 145–162.

Smith DO (1991). Sources of adenosine released during neuromuscular transmission in the rat. *J Physiol* **432**, 343–354.

Steinmeyer K, Klocke R, Ortland C, Gronemeier M, Jockusch H, Gründer S & Jentsch TJ (1991*a*). Inactivation of muscle chloride channel by transposon insertion in myotonic mice. *Nature* **354**, 304–308.

Steinmeyer K, Ortland C & Jentsch TJ (1991*b*). Primary structure and functional expression of a developmentally regulated skeletal muscle chloride channel. *Nature* **354**, 301–304.

Thomas SA & Hume RI (1993). Single potassium channel currents activated by extracellular ATP in developing chick skeletal muscle: a role for second messengers. *J Neurophysiol* **69**, 1556–1566.

Tricarico D, Camerino DC, Govoni S & Bryant SH (1991). Modulation of rat skeletal muscle chloride channels by activators and inhibitors of protein kinase C. *Pflugers Arch* **418**, 500–503.

van Emst MG, Klarenbeek S, Schot A, Plomp JJ, Doornenbal A & Everts ME (2004). Reducing chloride conductance prevents hyperkalaemia-induced loss of twitch force in rat slow-twitch muscle. *J Physiol* **561**, 169–181.

Vergara J, Tsien RY & Delay M (1985). Inositol 1,4,5-trisphosphate: a possible chemical link in excitation-contraction coupling in muscle. *Proc Natl Acad Sci U S A* **82**, 6352–6356.

Wells DG, Zawisa MJ & Hume RI (1995). Changes in responsiveness to extracellular ATP in chick skeletal muscle during development and upon denervation. *Dev Biol* **172**, 585–590.

Woo K, Dutta AK, Patel V, Kresge C & Feranchak AP (2008). Fluid flow induces mechanosensitive ATP release, calcium signalling and Cl^- transport in biliary epithelial cells through a PKCζ-dependent pathway. *J Physiol* **586**, 2779–2798.

Zifarelli G & Pusch M (2008). The muscle chloride channel ClC-1 is not directly regulated by intracellular ATP. *J Gen Physiol* **131**, 109–116.

Acknowledgements

All aspects of this work were completed in the UCLA David Geffen School of Medicine, Department of Physiology. The experiments were performed in the laboratory of Dr Julio Vergara. The author thanks Drs Julio Vergara and Ernest Wright for support and guidance for all aspects of this report. Importantly, a special note of thanks is given to Dr Donald Loo, who provided invaluable advice and discussions throughout the preparation of the manuscript. Additionally, the author is grateful to Drs Alan Grinnell, Yoshi Kidokoro, Marino DiFranco and Bruce Hirayama for numerous discussions and editorial comments; and Dr Baljit Khakh for outstanding experimental advice, equipment support and editorial comments. This work was supported by National Institutes of Health, NIDDK/NIAMS grant DK072818.